

The effect of an improved density functional on the thermodynamics and adsorption-controlled growth windows of chalcogenide perovskites

Stephen A. Filippone¹, Yi-Yang Sun,², R. Jaramillo^{1*}

- 1. Department of Materials Science and Engineering, Massachusetts Institute of Technology, 77 Massachusetts Ave., Cambridge, MA 02139, USA
- 2. State Key Laboratory of High Performance Ceramics and Superfine Microstructure, Shanghai Institute of Ceramics, Chinese Academy of Sciences, Shanghai 201899, China

Abstract

Ternary sulfides and selenides in the distorted-perovskite structure ("chalcogenide perovskites") are predicted by theory to be semiconductors with band gap in the visible-to-infrared and may be useful for optical, electronic, and energy conversion technologies. Density functional theory can be used in combination with computational thermodynamics to predict the pressure-temperature phase diagrams for chalcogenide perovskites. We report results using the Strongly Constrained and Appropriately Normed (SCAN) and the rVV10 density functionals, and compare to previously-published results using the PBEsol functional. We highlight the windows of thermodynamic equilibrium between solid chalcogenide perovskites and the vapor phase at high temperature and very low pressure. These phase diagrams can guide adsorption-limited growth of ternary chalcogenides by molecular beam epitaxy (MBE).

INTRODUCTION

Sulfides and selenides in the distorted-perovskite structure types (henceforth, simply called "chalcogenide perovskites") are an intriguing class of optoelectronic materials with mixed ionic-covalent bonding and band gap predicted to span from the visible to the infrared [1-3]. Interest in chalcogenide perovskites is increasing of late, led by theoretical studies of a wide range of $ABCh_3$ compositions (A = alkaline earth, B = transition metal, Ch = S or Se) and by experimental studies of powder samples including BaZrS₃, SrZrS₃, and CaZrS₃ [3-7]. An important next step in evaluating the optoelectronic

properties of chalcogenide perovskites is to grow large-grained thin films. To this end, we present temperature-pressure phase diagrams of *ACh-BCh*₂ pseudo-binary systems at ultrahigh vacuum (UHV) conditions. These phase diagrams can guide adsorption-limited growth of ternary chalcogenides by molecular beam epitaxy (MBE).

In a recent publication, we reported the phase diagrams for a number of $ABCh_3$ materials, using formation energies calculated by density functional theory (DFT) using the PBEsol functional [8]. Here we report the thermodynamics of $ABCh_3$ formation from binary chalcogenides using the recently-developed Strongly Constrained and Appropriately Normed (SCAN) and rVV10 density functionals, and the effect of these functionals on the pressure-temperature phase diagrams.

THEORY

The Strongly Constrained and Appropriately Normed (SCAN) functional was constructed to satisfy all currently known exact constraints on exchange, correlation functional and their sum [9]. The development of SCAN did not involve empirical fitting to a preselected dataset, and therefore the SCAN functional is considered to be fully non-empirical. The SCAN functional has been benchmarked to demonstrate its accuracy on the geometries and energies of diversely-bonded molecules and solids [10]. In particular, the functional handles well solids with diverse bonding types, including perovksites [10].

The rVV10 functional is designed to model layered materials with van der Waals bonding [11]. Some of the secondary phases considered here are *BCh*₂ layered transition metal di-chalcogenides with van der Waals bonding. Therefore, we have added the rVV10 functional to better calculate the formation energy of these competing, secondary phases.

RESULTS AND DISCUSSION

In Figure 1 and Table I we compare the enthalpy of formation of $ABCh_3$ from binary chalcogenides for compositions with A = (Ca, Sr, Ba), B = (Ti, Zr, Hf), and Ch = (S, Se). The $ABCh_3$ materials are all in the distorted perovskite phase with Pnma (#62) space group. The ACh and BCh_2 materials are in the rock-salt and 1T phases, respectively. The effect of adding the rVV10 functional to the SCAN functional is to systematically lower the formation enthalpy (ΔH_{form}): positive ΔH_{form} become less positive, and the negative ΔH_{form} become more negative.

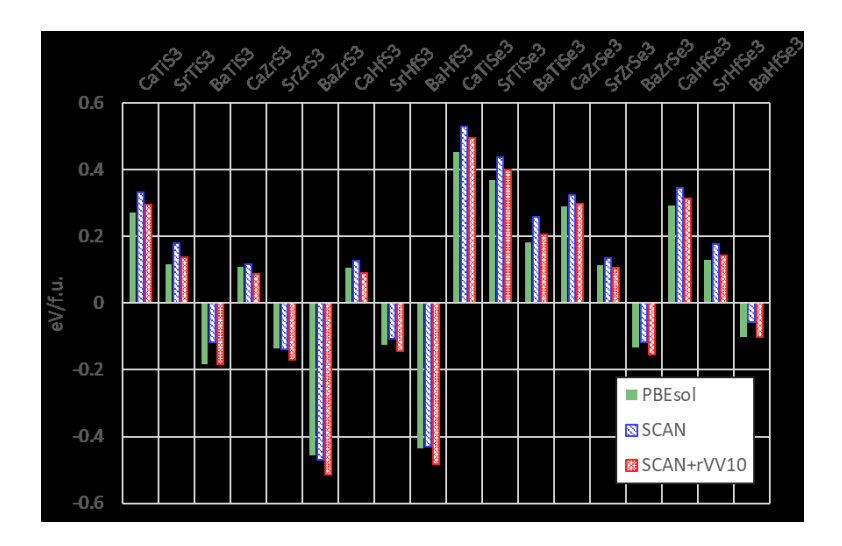


Figure 1: Enthalpy of formation of $ABCh_3$ chalcogenide perovskites from the binary chalcogenides ACh and BCh_2 calculated using different functionals: PBEsol = green, solid; SCAN = blue, diagonal lines; SCAN+rVV10 = red, hashed. Results are presented as energy in eV per formula unit (f.u.).

Table I: Enthalpy of formation of $ABCh_3$ chalcogenide perovskites from the binary chalcogenides ACh and BCh_2 calculated using different functionals. Results are presented as energy in eV per formula unit (f.u.).

Enthalpy of formation relative to binaries (eV/f.u.)						
Ternary	PBEsol	SCAN	SCAN+rVV10			
CaTiS3	0.270	0.331	0.296			
SrTiS3	0.116	0.179	0.137			
BaTiS3	-0.184	-0.118	-0.182			
CaZrS3	0.108	0.117	0.088			
SrZrS3	-0.135	-0.137	-0.169			
BaZrS3	-0.456	-0.470	-0.515			
CaHfS3	0.105	0.126	0.091			
SrHfS3	-0.125	-0.107	-0.144			
BaHfS3	-0.435	-0.429	-0.482			
CaTiSe3	0.453	0.529	0.496			
SrTiSe3	0.368	0.436	0.400			
BaTiSe3	0.181	0.257	0.206			
CaZrSe3	0.290	0.325	0.298			
SrZrSe3	0.114	0.134	0.106			
BaZrSe3	-0.133	-0.117	-0.154			
CaHfSe3	0.293	0.346	0.314			
SrHfSe3	0.129	0.176	0.142			
BaHfSe3	-0.103	-0.056	-0.101			

There is no clear trend explaining the difference between PBEsol and SCAN+rVV10 results. This is because the PBEsol functional yields reasonable interlayer distances for van der Waals-bonded transition metal dichalcogenides, even though it was not designed for such a purpose. In Table II we present the interlayer distance for *BCh*₂ calculated using all three approaches. The SCAN functional yields consistently larger lattice constants than PBEsol and SCAN+rVV10. Comparing to the experimental values tabulated in Peng *et al.*, we conclude that PBEsol and SCAN+rVV10 may be more reliable for semiconducting transition metal dichalcogenides (e.g. ZrS₂, ZrSe₂, HfS₂, and HfSe₂), but might overbind the vdW interaction in TiS₂ and TiSe₂, which are metallic [11].

Therefore, for compounds involving TiS_2 or $TiSe_2$ as secondary phases we prefer the results calculated with SCAN functional, while for other compounds the SCAN+rVV10 results may be more reliable.

 Table II: Inter-layer lattice constants (in Angstroms) for layered transition metal dichalcogenides calculated using different functionals. Experimental data are as tabulated in Peng et al. [11].

Binary	PBEsol	SCAN	SCAN+rVV10	Experiment
TiS2	5.61	5.91	5.62	5.90
TiSe2	5.92	6.24	6.00	6.27
ZrS2	5.86	6.01	5.77	5.81
ZrSe2	6.13	6.34	6.12	6.13
HfS2	5.90	6.01	5.77	5.84
HfSe2	6.17	6.33	6.12	6.16

We compute phase diagrams using the computational thermodynamics software package FactSage [12]. Briefly, we use the calculated enthalpy of formation and we estimate the (as-yet unmeasured) heat capacity of the $ABCh_3$ phases using the Neumann-Kopp rule. For details, please see our previous publication [8]. In Figure 2 we present the pressure-temperature phase diagrams under ACh-rich conditions for the six of the seven ACh- BCh_2 pseudo-binary systems for which the chalcogenide perovskite is calculated to be stable (negative $\Delta H_{\rm form}$). BaHfSe₃ is predicted to be stable, but we do not compute a phase diagram for the BaSe-HfSe₂ system because thermodynamic data are not available for HfSe₂.

On a pressure-temperature phase diagram, the thermodynamic growth window for a single-phase, compound solid film is a region in which the desired solid phase coexists with only the vapor phase. In this region, secondary solid phases are thermodynamically unstable, and the film growth rate is controlled by the adsorption of one binary component – this is also called adsorption-limited growth [8,13]. The growth windows for adsorption-limited growth of pure-phase $ABCh_3$ are labeled in Figure 2 as " $ABCh_3$ + vapor" for variable elements A, B, and Ch. We show growth windows in A-rich conditions; generally a growth window could also exist in B-rich conditions. However, the vapor pressure of the binary which is in excess will determine the upper bound of the growth window. Therefore, we choose the binary with the higher vapor pressure because this allows the most favorable process conditions. The use of more accurate functionals does not make an appreciable change to the phase diagrams. The growth windows remain narrow and experimentally inaccessible, where they exist at all. For instance, the BaS-ZrS₂ phase diagram predicts that adsorption-limited growth of BaZrS₃ would require precise control over pressure and temperature near 1000 °C and 10-9 Torr.

CONCLUSIONS

For $ABCh_3$ chalcogenide perovskites with A = alkaline earth and B = transition metal, the thermodynamic growth windows for adsorption-limited growth are experimentally daunting. Adsorption-limited growth of many $ABCh_3$ materials by MBE may require the development of high-vapor pressure precursors, as have been developed for the growth of ternary oxides by metal-organic MBE [14]. We note that many main group binary chalcogenides have high vapor pressure, which may permit the adsorption-limited MBE growth of $ABCh_3$ materials with main group elements B using metal sources.

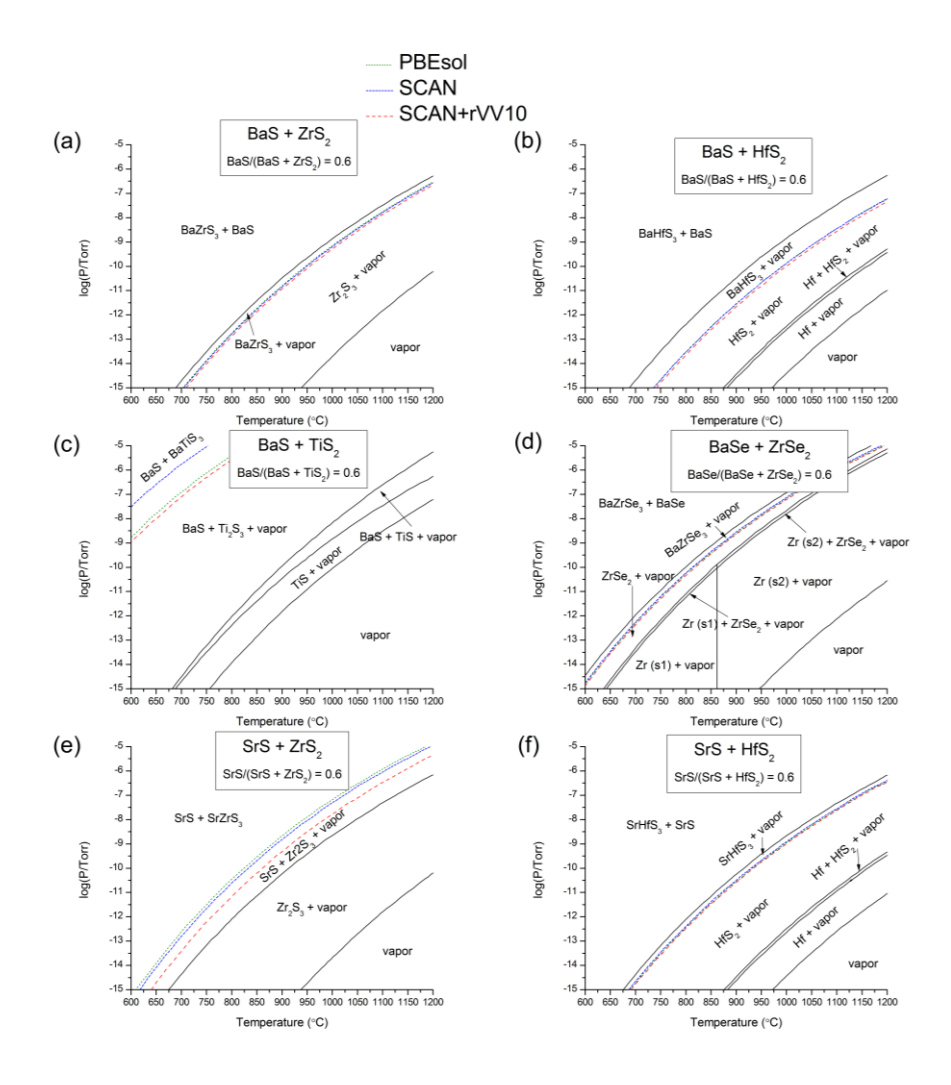


Figure 2: Temperature-pressure phase diagrams for six of the chalcogenide perovskites that are calculated to be thermodynamically stable relative to decomposition into binary chalcogenides. The fixed composition in each case is a mole fraction of 0.6 of the ACh component. The pressure is the sum of the partial pressures of all gas species in the system. In each case, the thermodynamic growth window is labeled " $ABCh_3$ + vapor" for variable elements A, B, and Ch. The calculated enthalpy of formation affects the lower bound of the growth window, if such exists. We show results for calculations using three different functionals, with the corresponding lines indicated by color according to the legend above: PBEsol = green, short dashes; SCAN = blue, longer dashes; SCAN+rVV10 = red, widely-spaced dashes. (a) BaS-ZrS₂ system. (b) BaS-HfS₂ system. (c) BaS-TiS₂ system. (d) BaSe-ZrSe₂ system. (e) SrS-ZrS₂ system. (f) SrS-HfS₂ system.

ACKNOWLEDGEMENTS

Stephen A. Filippone acknowledges support from the National Science Foundation Graduate Research Fellowship under Grant No. 1122374. Y.-Y. S. acknowledges support from National Natural Science Foundation of China under Grant

No. 11774365. This project was funded in part by the MIT Skoltech Seed Fund, as part of the MIT Skoltech Program.

REFERENCES

- ¹ J.W. Bennett, I. Grinberg, and A.M. Rappe, Phys. Rev. B **79**, 235115 (2009).
- ² J.A. Brehm, J.W. Bennett, M.R. Schoenberg, I. Grinberg, and A.M. Rappe, J. Chem. Phys. **140**, 224703 (2014).
- ³ Y.-Y. Sun, M.L. Agiorgousis, P. Zhang, and S. Zhang, Nano Lett. 15, 581 (2015).
- Y.-Y. Sun, M.L. Agiorgousis, P. Zhang, and S. Zhang, Nano Lett. 15, 581 (2015).
 S. Perera, H. Hui, C. Zhao, H. Xue, F. Sun, C. Deng, N. Gross, C. Milleville, X. Xu, D.F. Watson, B. Weinstein, Y.-Y. Sun, S. Zhang, and H. Zeng, Nano Energy 22, 129 (2016).
 W. Meng, B. Saparov, F. Hong, J. Wang, D.B. Mitzi, and Y. Yan, Chem. Mater. 28, 821 (2016).
 S. Niu, H. Huyan, Y. Liu, M. Yeung, K. Ye, L. Blankemeier, T. Orvis, D. Sarkar, D.J. Singh, R. Kapadia, and J. Ravichandran, Adv. Mater. 29, 1604733 (2017).
 M.-G. Ju, J. Dai, L. Ma, and X.C. Zeng, Adv. Energy Mater. 7, 1700216 (2017).
 S.A. Filippone, Y.-Y. Sun, and R. Jaramillo, MRS Commun. 1 (2018).
 J. Sun, A. Ruzsinszky, and J.P. Perdew, Phys. Rev. Lett. 115, 036402 (2015).
 J. Sun, R.C. Remsing, Y. Zhang, Z. Sun, A. Ruzsinszky, H. Peng, Z. Yang, A. Paul, U. Waghmare, X. Wu, M.L. Klein, and J.P. Perdew, Nat. Chem. 8, 831 (2016).
 H. Peng, Z.-H. Yang, J.P. Perdew, and J. Sun, Phys. Rev. X 6, 041005 (2016).
 C.W. Bale, E. Bélisle, P. Chartrand, S.A. Decterov, G. Eriksson, A.E. Gheribi, K. Hack, I.-H. Jung, Y.-B. Kang, J. Melancon, A.D. Pelton, S. Petersen, C. Robelin, J. Sangster, P.

- Jung, Y.-B. Kang, J. Melançon, A.D. Pelton, S. Petersen, C. Robelin, J. Sangster, P.
- Spencer, and M.-A. Van Ende, Calphad **54**, 35 (2016).

 ¹³ J.Y. Tsao, *Materials Fundamentals of Molecular Beam Epitaxy*, 1 edition (Academic Press,
- Boston, 1992).

 14 M. Henini, editor, Molecular Beam Epitaxy: From Research to Mass Production, 1st ed. (Elsevier, 2012).